

## Article

# Durability-Aimed Design Criteria of Cement-Stabilized Loess Subgrade for Railway

Fuyu Wang <sup>1</sup>, Weichen Pang <sup>1</sup>, Xingyuan Qin <sup>1</sup>, Leilei Han <sup>1,\*</sup>  and Yingjun Jiang <sup>2</sup>

<sup>1</sup> School of Transportation, Jilin University, Changchun 130022, China; wfy@jlu.edu.cn (F.W.); pangwc19@mails.jlu.edu.cn (W.P.); xingyuant20@mails.jlu.edu.cn (X.Q.)

<sup>2</sup> Key Laboratory for Special Area Highway Engineering of Ministry of Education, Chang'an University, Xi'an 710064, China; jyj@chd.edu.cn

\* Correspondence: hanll18@mails.jlu.edu.cn

**Abstract:** The subgrade is the foundation of railway construction, so its strength and stability are very important to ensure the safety and stability of a train. Loess is widely distributed in northwestern China, and it must be stabilized before being used in railway subgrade construction because loess is sensitive to water. Railway subgrade withstands not only the train load but also repeated attacks from the environment and climate because it has to be exposed to natural environment after construction. Therefore, the strength of cement-stabilized loess deteriorates continuously because of the above factors. Taking account of long-term stability, the influences of load on the cement-stabilized loess as well as the strength reduction laws of cement-stabilized loess under wet–dry cycling and freeze–thaw cycling were analyzed in this study. Additionally, the respective reduction coefficients were obtained. Finally, the strength design criteria of cement-stabilized loess subgrade were put forward based on railway subgrade durability by analyzing the obtained reduction coefficients and the critical dynamic strength of railway subgrade.



**Citation:** Wang, F.; Pang, W.; Qin, X.; Han, L.; Jiang, Y. Durability-Aimed Design Criteria of Cement-Stabilized Loess Subgrade for Railway. *Appl. Sci.* **2021**, *11*, 5061. <https://doi.org/10.3390/app11115061>

Academic Editor: Daniel Dias

Received: 6 May 2021

Accepted: 25 May 2021

Published: 30 May 2021

**Publisher's Note:** MDPI stays neutral with regard to jurisdictional claims in published maps and institutional affiliations.



**Copyright:** © 2021 by the authors. Licensee MDPI, Basel, Switzerland. This article is an open access article distributed under the terms and conditions of the Creative Commons Attribution (CC BY) license (<https://creativecommons.org/licenses/by/4.0/>).

**Keywords:** loess; strength; wet–dry cycling; freeze–thaw cycling; design criteria

## 1. Introduction

Loess has good strength and high compressive resistance, which has been widely used in the construction of railway subgrade. However, loess is sensitive to water, so it is prone to significant deformation and settlement after being immersed in water. Cement is usually used to improve the characteristics of loess [1–4]. Besides, innovative recycled materials such as plastic and glass have been used in railway substructure [5,6]. The strength of cement-stabilized loess gradually deteriorates under the action of wet–dry cycling, freeze–thaw cycling and repeated load because railway subgrade is exposed to the natural environment. Therefore, when designing the railway subgrade filling, the impact of environment and the train load on the subgrade should be considered to ensure the long-term strength, stability and durability of the subgrade.

At present, as for stabilized soil, many engineering departments use unconfined compressive strength  $q_u$  as the strength index in China and other countries [7–9]. The actual experience of railway departments in China shows that it is safer to choose 7-day saturation strength as the strength of stabilized soil [10]. As for the durability of subgrade, many countries refer to the loss rate of mass or strength after 12 times of wet–dry and freeze–thaw cycling, according to the ASTM (American Society for Testing Material). However, the loss rate of strength after only 5 times of wet–dry and freeze–thaw cycling is used to control the durability of subgrade in China [11], and long-term stability under influences of wet–dry and freeze–thaw cycling is less considered. The strength design criteria of stabilized soil of subgrade bottom and embankment below the subgrade of all grades of the railway are shown in Table 1, which is provided by “Code for Design of Railway Earth Structure” [12].

**Table 1.** The strength requirement of stabilized soil in China.

The Grade of Railway		Design Speed (km/h)	7-Day Unconfined Compressive Strength Saturated with Water (kPa)	
			Subgrade Bottom	Embankment below the Subgrade
Passenger and freight railway, Inter-city railway	Ballast track	120, 160	≥350 (550)	≥200
		200	≥350 (550)	≥250
	Ballastless track	-	≥350 (550)	≥250
High-speed railway, Heavy-haul railway		-	≥350 (550)	≥250

Note: The contents in brackets refer to the strength value of stabilized soil considering freeze–thaw cycling.

In this study, several inter-city railways in Shaanxi, China, were selected for testing. The first selected loess was not immersed in water with a compaction level of 90%. Its minimum unconfined compressive strength was 420 kPa, which is 1.20 times the required critical strength (350 kPa) of the subgrade bottom. The second selected 8 types of cement-stabilized loess were saturated with water with 90% compaction level and 3% cement dosage. Its minimum 7-day unconfined compressive strength was 514 kPa, which is 1.47 times the required critical strength of the subgrade bottom. It can be seen that the design criteria in Table 1 cannot control the construction quality very well.

In fact, the design criteria of filling can be determined by Equation (1) based on strength control.

$$[q_u] \geq \sigma_{dmax} \quad (1)$$

$$[q_u] = k_f \times \eta_G \times \eta_D \times q_u \quad (2)$$

where

$[q_u]$  is the strength considering the impact of the environment and train load on the subgrade filling, kPa;

$q_u$  is the strength without the impact of the environment and train load on the subgrade filling, kPa;

$\sigma_{dmax}$  is the maximum dynamic stress of subgrade, kPa;

$k_f$  is the fatigue reduction coefficient of the subgrade filling under repeated train load;

$\eta_G$  is the strength reduction coefficient of the subgrade filling under wet–dry cycling;

$\eta_D$  is the strength reduction coefficient of the subgrade filling under freeze–thaw cycling.

The strength design criterion  $q_u$  of subgrade filling can be obtained by substituting Equation (2) into Equation (1).

$$q_u \geq \sigma_d / (k_f \cdot \eta_G \cdot \eta_D) \quad (3)$$

Two aspects should be considered when determining the strength design criteria of subgrade filling for the railway. One is  $\sigma_{dmax}$ , and the other is  $\eta_G$  and  $\eta_D$ . For dynamic stress, Zhu et al. investigate dynamic compressive stress characteristics and related influencing factors in the permafrost site along Qinghai–Tibet Railway [13]. Yao et al. presented a full vehicle–track–ground coupling model to evaluate the dynamic response of subgrade due to high-speed trains [14]. Wang et al. compared the dynamic responses of the earth structures constructed using stabilized cinders and traditional geomaterials [15]. Ma et al. conducted the dynamic triaxial tests on cement- and lime-improved loess specimens to study the cyclic shear strain threshold and critical dynamic stress [16]. Fang et al. established a new track–multilayer ground model to investigate railway subgrade dynamic responses induced by moving train load [17]. Moreover, dynamic responses of high-speed railway and heavy-haul railway were studied by some scholars [18–24]. In China, Ye et al. studied the subgrade design indices of improved soil and found that the cumulative deformation rate of stabilized soil was less than 0.5% when the strength of improved soil was 5 times the critical dynamic strength of filling [25]. Based on theoretical calculation

and field measurement data, the strength design criteria of filling can be 250 kPa of the top surface of the subgrade bottom and 125 kPa of embankment below the subgrade bottom when the design values of dynamic stress are 50 kPa and 25 kPa, respectively, and the actual design criteria are 416 kPa and 208 kPa because of the differences between field and laboratory, which is basically consistent with Table 1 [26–36].

As for train loads, Fahoum et al. studied the fatigue stability of cement-stabilized soil under a cyclic load of the train [37]. Preteseille et al. pointed that the selection and design of filling are closely related to fatigue performance, which can avoid empirical errors [38]. Lenior et al. studied the fatigue performance of fiber-cement-stabilized soil and found that the fatigue performance of cement-stabilized soil-doped fiber was improved [39].

As for environmental factors, the effects of wet–dry cycling and freeze–thaw cycling on loess and stabilized loess were studied [40–46]. Yan et al. investigated the characteristics of unconfined compression strength and void distribution of lime–flyash loess by means of a series of experiments under freeze–thaw cycling or wet–dry cycling [47]. Besides, Yan et al. studied the reduction law of the antierosion ability parameters of PP fiber-reinforced loess under wet–dry cycling and freeze–thaw cycling [48]. Hu et al. established a compacted loess reduction model that comprehensively considers the influencing factors [49]. Zhang et al. studied the influence of cement dosage and water content on the compressive strength of cement-stabilized soil under wet–dry cycling and found that cement dosage is the decisive factor to affect the durability of wet–dry resistance of cement-stabilized soil [50]. Helson et al. studied the mass change of cement-stabilized soil under wet–dry cycling [51]. Zhao et al. studied the shearing strength characteristics of cement-stabilized soil under freeze–thaw cycling [52].

In view of the required values being too low to be better used for engineering control due to defective consideration of strength reduction of cement-stabilized loess under wet–dry cycling, freeze–thaw cycling in current criteria in China, the strength design criteria of cement-stabilized loess combined the above factors were investigated in this study. Firstly, the strength reduction coefficients of cement-stabilized loess were calculated under train load, wet–dry cycling and freeze–thaw cycling. Additionally, the dynamic stress of the railway subgrade and the critical dynamic strength of filling were analyzed. After that, the values of each index in Equation (3) could be determined. Finally, the strength design criteria were presented after a comprehensive analysis.

## 2. Experimental Design

### 2.1. Materials

#### 2.1.1. Loess

The physical properties of loess used in this study are shown in Table 2. The loess was collected from the area where the Xi’an-Hancheng inter-city railway is located. The appearance of the loess is bright yellow and loose. The type of the loess is silty clay, and the depth is about 3 m.

**Table 2.** Physical properties of loess.

Technical Indices	Particle Density (g/cm <sup>3</sup> )	Liquid Limit (%)	Plastic Limit (%)	Plasticity Index	Percentage Passing (%) of Sieve Sizes (mm)				
					0.25~0.075	0.075~0.05	0.05~0.01	0.01~0.005	≤0.005
Test value	2.74	26.4	15.7	10.7	2.47	7.22	53.43	13.83	23.05

#### 2.1.2. Cement

The technical properties of cement for performance tests are shown in Table 3, which was P.O42.5 ordinary Portland cement.

## 2.2. Specimens Preparation

The optimum moisture content and the maximum dry density of cement-stabilized loess with each cement dosage were determined according to the heavy compaction test from the “Code for Soil Test of Railway Engineering” [53]. The specimens were prepared by static pressure method, and the prepared specimens were placed in a curing room with a temperature of  $20 \pm 2$  °C and a humidity of 95% until 24 h before the specified curing time.

**Table 3.** Technical properties of cement.

Technical Indices	Fineness (%)	Soundness	Ignition Loss (%)	Initial Setting Time (min)	Final Setting Time (min)
Testing standard	$\leq 10$	Qualified	$\leq 5$	$\geq 45$	$\leq 600$
Test value	1.2	Qualified	1.02	265	320

Different cement dosages were used to study the strength reduction coefficient of cement-stabilized loess influenced by wet–dry cycling, freeze–thaw cycling and load. The cement dosages were 2%, 3%, 4% and 6%, respectively. The influences of wet–dry cycling and freeze–thaw cycling on the strength of cement-stabilized loess were studied. Various compaction levels were conducted, which are 0.92, 0.95 and 0.97, respectively.

## 2.3. Test Methods

### 2.3.1. Fatigue Test

The fatigue test using the indirect tension method was chosen in this study. The mode was stress control, and the load was a sinusoidal wave. The cyclic characteristic coefficient  $R$  (maximum and minimum stress ratio) was 0.1 [54], the 5 stress levels  $S$  were 0.85, 0.80, 0.75, 0.70 and 0.65, and the load frequency was 4 Hz. The material testing system (MTS-810) was used for the test, and the setup of the specimen is shown in Figure 1.



**Figure 1.** The setup of specimen.

### 2.3.2. Wet-Dry Cycling

The specimens were immersed in water at a temperature of  $20 \pm 2$  °C for 24 h and divided into 2 groups. Specimens from the first group were tested according to the wet–dry cycling test method [55]. Then, the unconfined compressive strength of all specimens were tested according to the method of TB10102 [53]. The unconfined compressive strength without wet–dry cycling was denoted by  $q_u$ , and the unconfined compressive strength with  $n$  times of wet–dry cycling was denoted by  $q_G$ .

### 2.3.3. Freeze-Thaw Cycling

The freeze–thaw cycling was conducted according to T0858 of “Test Methods of Materials Stabilized with Inorganic Binders for Highway Engineering” [56]. The specimens were immersed in water at a temperature of  $20 \pm 2$  °C for 24 h and divided into two groups.

Specimens from the first group were performed  $n$  times of freeze–thaw cycling. Then, the unconfined compressive strength of all specimens was tested according to the method of TB 10102 [53]. The unconfined compressive strength without freeze–thaw cycling was denoted by  $q_u$ , and the unconfined compressive strength with  $n$  times of freeze–thaw cycling was denoted by  $q_{Du}$ .

### 3. Results and Discussion

#### 3.1. Fatigue Performance of Cement-Stabilized Loess

The fatigue test results of cement-stabilized loess are shown in Table 4. According to previous studies, the Weibull distribution was used to analyze and process the above data [57]. The fatigue life  $N$  and the equivalent fatigue life  $\bar{N} (\bar{N} = N^{1-R})$  of cement-stabilized loess obey a two-parameter Weibull distribution, and then the failure probability  $\rho$  is [58]:

$$\rho = F(\bar{N}) = 1 - \exp \left[ -(\bar{N}/t_0)^m \right], N \geq 1; m, t_0 > 0 \tag{4}$$

where

- $m$  is shape parameter;
- $t_0$  is scale parameter.

**Table 4.** The fatigue test results of cement-stabilized loess.

Cement Dosage, $P_s$ (%)	Compaction Level (K)	The Fatigue Life $N$ of Cement-Stabilized Loess Specimens under the Following Stress Levels $S$ (Time)				
		0.80	0.75	0.70	0.65	0.60
3	0.92	239	568	1326	4825	8143
		344	782	2072	6843	11,629
		656	996	2945	8848	14,401
		897	1453	4177	10,268	19,955
		1121	1882	5584	12,851	26,785
	0.95	416	1645	4060	9061	19,320
		688	3098	7345	16,453	34,396
		935	4552	8840	23,697	46,005
		1210	6009	11,285	32,078	54,720
		1720	7946	13,865	42,153	72,153
	0.97	578	3177	6835	13,645	51,421
		896	4945	9275	22,787	76,553
		1427	6362	12,951	30,597	85,648
		2166	7761	15,784	35,780	100,990
		3439	9581	17,896	49,668	121,764
4	0.92	389	895	2846	8815	10,524
		536	1539	3781	10,629	13,066
		861	2262	4974	13,815	17,251
		1062	3122	5655	15,993	21,892
		1413	4528	7523	18,651	24,145
	0.95	575	3628	7225	15,729	40,548
		906	5043	9356	28,955	53,526
		1288	6215	13,023	35,726	67,262
		1662	8149	14,898	44,830	81,049
		2141	9352	17,653	56,004	89,553
	0.97	810	5682	11,617	36,299	78,219
		1621	7427	18,528	54,473	90,316
		2577	8932	26,743	60,338	99,886
		3705	10,055	34,622	72,455	114,190
		5106	11,947	43,850	81,637	130,925

Table 4. Cont.

Cement Dosage, $P_s$ (%)	Compaction Level (K)	The Fatigue Life $N$ of Cement-Stabilized Loess Specimens under the Following Stress Levels $S$ (Time)				
		0.80	0.75	0.70	0.65	0.60
6	0.92	541	1676	4571	11,259	82,150
		809	3587	7033	18,215	101,583
		1168	4633	9124	31,945	134,783
		1382	5684	13,086	39,661	159,745
		2033	7590	17,258	50,157	181,738
	0.95	763	4781	10,273	61,235	125,681
		1256	6955	15,831	97,650	165,240
		1864	9271	20,773	116,042	228,132
		3295	11,352	23,896	158,123	273,185
		4136	13,161	31,652	195,635	325,160
	0.97	970	7195	21,453	101,887	162,293
		1954	10,862	32,612	145,064	230,919
		2766	14,276	43,965	204,692	292,588
		4081	21,016	51,432	287,654	345,067
		4852	26,422	60,100	346,950	423,740

Assuming that there is a fatigue limit of cement-stabilized loess, the fatigue equation should satisfy the following two boundary conditions:

- when  $S = 1, N = 1$ ;
- when  $S = 0, N \rightarrow \infty$ ;

The above boundary conditions are properly relaxed to obtain a relatively reasonable fatigue equation, which is Equation (5).

$$\lg N = m - n \lg S \tag{5}$$

where

$m$  and  $n$  are undetermined regression coefficients of the fatigue equation.

According to Equations (4) and (5), the data in Table 4 were analyzed to obtain the fatigue prediction equation of cement-stabilized loess with a 5% failure probability. The results are shown in Table 5.

Table 5. Prediction equation regression coefficient of fatigue life  $N$  of cement-stabilized loess.

$P_s$ (%)	3			4			6			Average
	K	0.92	0.95	0.97	0.92	0.95	0.97	0.92	0.95	
$m$	0.571	1.062	0.780	0.823	1.125	0.890	0.591	0.679	0.883	0.823
$n$	14.393	13.667	17.253	14.543	15.368	18.426	17.864	19.806	19.666	16.776
$R^2$	0.9662	0.9706	0.9378	0.9356	0.9378	0.9268	0.9663	0.9540	0.9542	

According to a 0.95 confidence level, the regression coefficient of the fatigue equation of cement-stabilized loess was calculated, which is shown in Equations (6) and (7).

$$m_{0.95} = \bar{m} - 1.645S \tag{6}$$

$$n_{0.95} = \bar{n} - 1.645S \tag{7}$$

where

$\bar{m}$  and  $\bar{n}$  are the average of undetermined regression coefficients of the fatigue equation;  $S$  is the criteria deviation.

The fatigue reduction coefficient is used to represent the strength reduction characteristics of specimens after repeated load. According to the above research, the fatigue reduction coefficient  $k_f$  of cement-stabilized loess could be expressed as:

$$k_f = \sqrt[n]{10^m / N_e} \tag{8}$$

where

$N_e$  is the accumulated times of axle load within the design life.

It was assumed that railway capacity is saturated, the daily running capacity of trains is 90, and the number of accumulated daily axle load is 2880 [59,60]. Then, the cumulative number of axle loads in the design life  $N_e$  is  $1.05 \times 10^8$  times. The fatigue reduction coefficient  $k_f$  of cement-stabilized loess is 0.262 when  $m_{0.95}$ ,  $n_{0.95}$  and  $N_e$  are substituted into Equation (8). This result is overall consistent with the principle that the critical strength of improved soil is 5 times the dynamic stress [25]. Therefore, the fatigue reduction factor  $k_f$  of cement-stabilized loess is 0.26 in this study.

### 3.2. Strength Reduction under Wet-Dry Cycling

The 28-day compressive strength test results of cement-stabilized loess under wet–dry cycling are shown in Table 6. The wet–dry reduction coefficient is used to represent the reduction characteristics of compressive strength of specimens after wet–dry cycling, which was calculated according to Equation (9). The greater the wet–dry reduction coefficient, the smaller the strength reduction of stabilized loess after wet–dry cycling.

$$\eta_G = q_G / q_u \tag{9}$$

where

$\eta_G$  is the strength reduction coefficient under wet–dry cycling;

$q_G$  is the compressive strength of specimens after  $N$  times of wet–dry cycling;

$q_u$  is the compressive strength of specimens before wet–dry cycling.

**Table 6.** The 28-day compressive strength test results of cement-stabilized loess under wet–dry cycling.

Cement Dosage, $P_s$ (%)	Compaction Level (K)	The Compressive Strength (MPa) of Cement-Stabilized Loess under the Following Cycling $N$ (Time)									
		0	1	3	5	7	9	12	15	20	25
2	0.92	1.03	0.73	0.68	0.58	0.53	0.48	0.44	0.43	0.43	0.43
	0.95	1.34	1.06	0.91	0.80	0.72	0.66	0.60	0.58	0.58	0.56
	0.97	1.65	1.32	1.14	1.01	0.91	0.83	0.76	0.73	0.73	0.71
3	0.92	1.30	1.03	0.88	0.75	0.69	0.64	0.57	0.55	0.55	0.55
	0.95	1.60	1.28	1.10	0.99	0.86	0.82	0.74	0.70	0.69	0.69
	0.97	2.03	1.68	1.44	1.28	1.12	1.08	0.95	0.89	0.89	0.89
4	0.92	1.49	1.21	1.04	0.94	0.83	0.76	0.69	0.64	0.64	0.63
	0.95	1.90	1.58	1.39	1.24	1.08	0.99	0.91	0.84	0.84	0.84
	0.97	2.26	1.90	1.74	1.56	1.29	1.24	1.11	1.02	1.01	1.01
6	0.92	2.03	1.68	1.42	1.30	1.14	1.04	0.95	0.87	0.87	0.87
	0.95	2.44	2.03	1.78	1.63	1.39	1.27	1.17	1.07	1.06	1.05
	0.97	2.80	2.38	2.18	1.96	1.62	1.60	1.34	1.26	1.25	1.25

Assuming that there is a strength reduction coefficient equation for cement-stabilized loess under wet–dry cycling, and it is satisfied the following three boundary conditions:

$$\text{when } N = 0, \eta_{GN} = \eta_{G0}$$

$$\text{when } N = \infty, \eta_{GN} = \eta_{G\infty}$$

$$\eta_{G0} > \eta_{G\infty}$$

where

$N$  is the time of wet–dry cycling of cement-stabilized loess;

$\eta_{GN}$  is the strength reduction coefficient of cement-stabilized loess after  $N$  times of wet–dry cycling;

$\eta_{G0}$  is the strength reduction coefficient of cement-stabilized loess before wet–dry cycling, which is equal to 1;

$\eta_{G\infty}$  is the limit of strength reduction coefficient of cement-stabilized loess under wet–dry cycling.

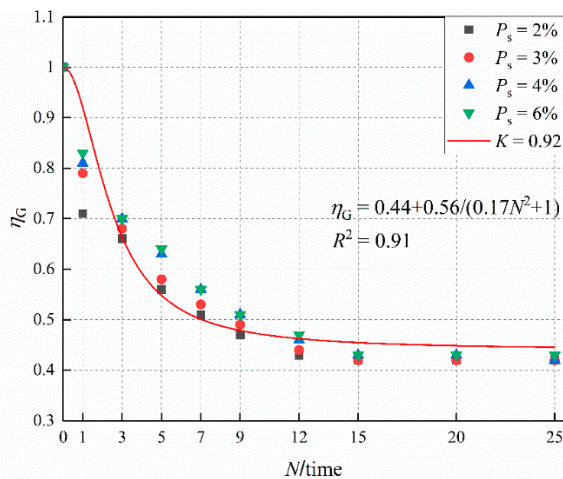
According to the above boundary conditions, the strength reduction coefficient equation of cement-stabilized loess after wet–dry cycling was established:

$$\eta_{GN} = \eta_{G\infty} - (\eta_{G\infty} - 1) / (\zeta \cdot N^2 + 1) \tag{10}$$

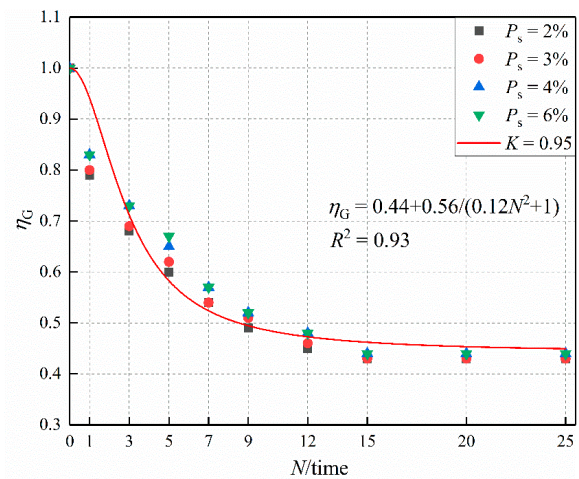
where

$\zeta$  is the regression parameter of equation.

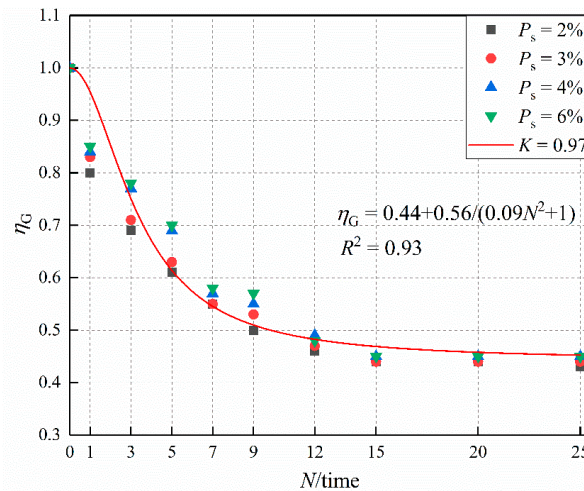
The strength reduction coefficient equations of cement-stabilized loess after wet–dry cycling were obtained by fitting with Equation (10), which are shown in Figure 2. As can be seen from Figure 2, the strength reduction of cement-stabilized loess gradually increases with the increase of the number of wet–dry cycling, and the reduction coefficient is stable between 0.41 and 0.48 after more than 15 times of wet–dry cycling. According to the most unfavorable conditions, the reduction coefficient of cement-stabilized loess under wet–dry cycling is 0.4.



(a)  $K = 0.92$



(b)  $K = 0.95$



(c)  $K = 0.97$

Figure 2. The relationship between  $\eta_G$  and  $N$ .

### 3.3. Strength Reduction under Freeze-Thaw Cycling

The compressive strength test results of cement-stabilized loess under freeze–thaw cycling are shown in Table 7. The specimens with 2% of dosage became loose after 10 freeze–thaw cycles, so these data were not recorded. The freeze–thaw reduction coefficient is used to represent the reduction characteristics of compressive strength of specimens after freeze–thaw cycling, which was calculated according to Equation (11). The greater the freeze–thaw reduction coefficient, the smaller the strength reduction of stabilized loess after freeze–thaw cycling.

$$\eta_D = q_{Du} / q_u \tag{11}$$

where

- $\eta_D$  is the strength reduction coefficient under freeze–thaw cycling;
- $q_{Du}$  is the compressive strength of specimens after  $N$  times of freeze–thaw cycling;
- $q_u$  is the compressive strength of specimens before freeze–thaw cycling.

**Table 7.** The 28-day compressive strength test results of cement-stabilized loess under freeze–thaw cycling.

Cement Dosage, $P_s$ (%)	Compaction Level (K)	The Compressive Strength (MPa) of Cement-Stabilized Loess under the Following Cycling $N$ (Time)								
		0	1	3	5	7	9	12	15	20
2	0.92	1.03	0.71	0.61	0.46	0.31	0.24	-	-	-
	0.95	1.34	0.96	0.81	0.62	0.43	0.29	-	-	-
	0.97	1.65	1.22	1.01	0.80	0.57	0.39	-	-	-
3	0.92	1.30	0.95	0.81	0.64	0.49	0.42	0.39	0.37	0.37
	0.95	1.60	1.19	1.04	0.81	0.71	0.64	0.60	0.58	0.57
	0.97	2.03	1.53	1.32	1.05	0.93	0.84	0.78	0.75	0.75
4	0.92	1.49	1.13	0.98	0.76	0.64	0.58	0.53	0.52	0.52
	0.95	1.90	1.44	1.28	1.02	0.90	0.83	0.77	0.75	0.74
	0.97	2.26	1.76	1.55	1.30	1.11	1.02	0.96	0.93	0.93
6	0.92	2.03	1.56	1.37	1.05	0.91	0.83	0.76	0.74	0.74
	0.95	2.44	1.89	1.61	1.32	1.16	1.05	0.99	0.98	0.98
	0.97	2.80	2.18	1.87	1.59	1.38	1.23	1.16	1.14	1.14

The strength reduction coefficient equation of cement-stabilized loess after freeze–thaw cycling is established with the same method in Section 3.2.

$$\eta_{DN} = \eta_{D\infty} - (\eta_{D\infty} - 1) / (\xi \cdot N^2 + 1) \tag{12}$$

where

- $\eta_{DN}$  is the strength reduction coefficient of cement-stabilized loess after  $N$  times of freeze–thaw cycling;
- $\eta_{D\infty}$  is the limit of strength reduction coefficient of cement-stabilized loess under freeze–thaw cycling.
- $N$  is the time of freeze–thaw cycling of cement-stabilized loess;
- $\xi$  is the regression parameter of the equation.

The strength reduction coefficient equations of cement-stabilized loess after freeze–thaw cycling was obtained by fitting with Equation (12), which are shown in Figure 3. As can be seen from Figure 3, the strength reduction of cement-stabilized loess gradually increases with the increase of the number of freeze–thaw cycles, and the reduction coefficient is stable between 0.33 and 0.40 after more than 12 times of freeze–thaw cycling.

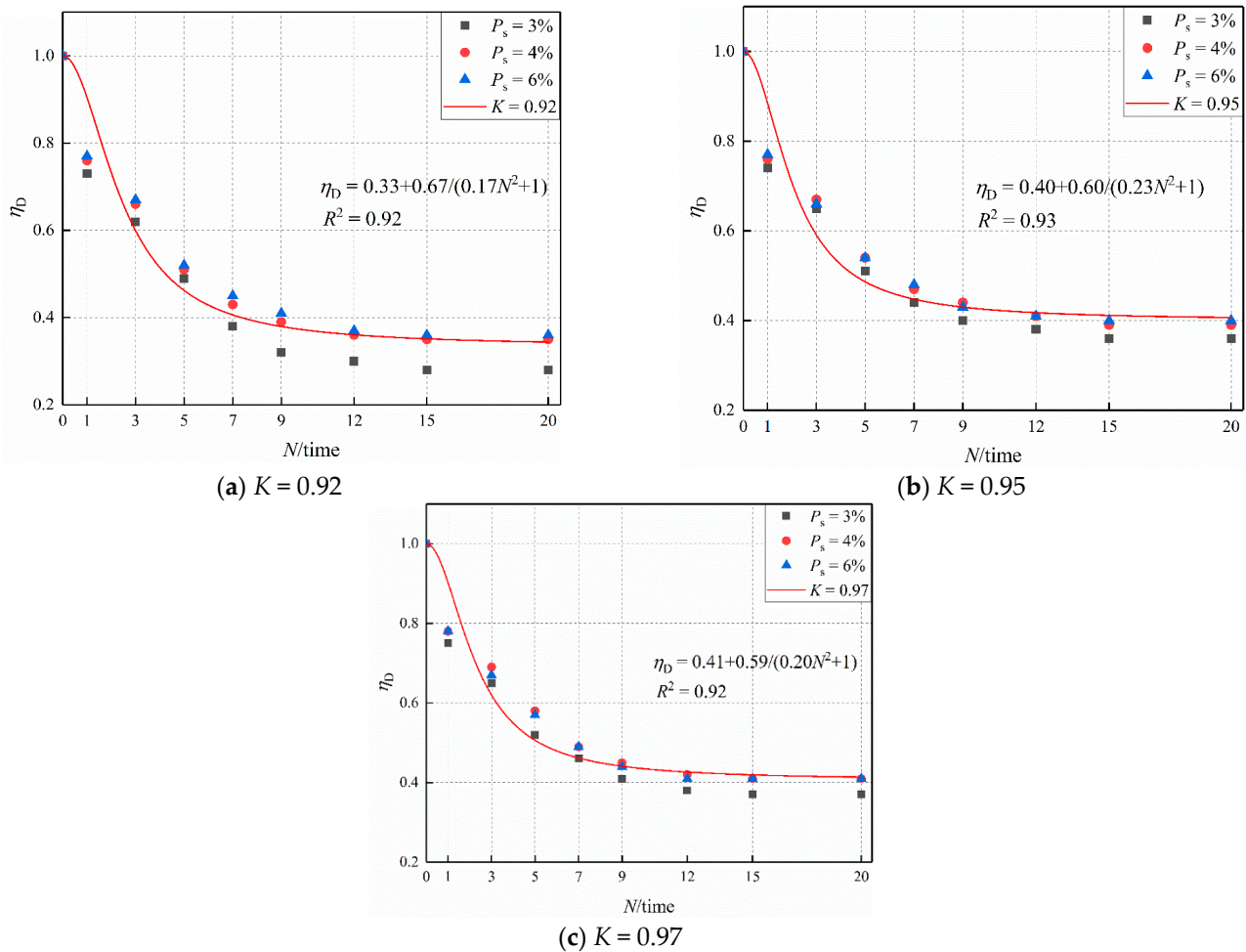


Figure 3. The relationship between  $\eta_D$  and  $N$ .

The average permafrost depth in Xi’an, Chengcheng and Hancheng, China, is 45 cm, 29.6 cm and 19 cm, respectively, during 28 years, and the extreme depth of permafrost in northwestern China can reach more than 80 cm [61,62]. Therefore, the reduction coefficient of the freeze–thaw cycling is 0.3 according to the most unfavorable conditions.

#### 4. The Design Criteria Aiming at Subgrade Durability

##### 4.1. Determination of Dynamic Stress

The strength control method is usually used to determine the thickness of the railway subgrade bed and material strength, which is the maximum dynamic stress  $\sigma_{dmax}$  transferred to filling through the subgrade bed under the train load must be less than the allowable strength of filling.

As for measured values of dynamic stress, there is a belief that that the dynamic response of the existing railway subgrade was 35.0~86.0 kPa in China [63]. In addition, the dynamic stress of some specific test sections of the railway was specially tested by some Chinese scholars [27,31,64–67]. The study showed that the dynamic stress of subgrade surface does not change significantly with train speed but increases with the increase of axle load [68]. As for the calculated value of dynamic stress, the formula of the maximum dynamic stress  $\sigma_{max}$  of subgrade surface was given in “Code for Design of Intercity Railway” [69] and “Code for Design of High Speed Railway” [70]. In addition to the criteria, some scholars calculated the dynamic stress by finite element simulation [31,32]. It was found that the calculated values are in good agreement with the measured values. It can verify the possibility of finite element analysis. The measured and theoretical data showed that the dynamic stress of the subgrade decreases rapidly with depth [26–36]. As for the

reduction law of dynamic stress along the depth, it can be known that the calculated value of dynamic stress of subgrade is generally greater than the measured value according to the above research results. Based on the existing research results, it was determined that the dynamic stress of the subgrade bottom is 20–50 kPa, and the dynamic stress of embankment below the subgrade bottom is 10–25 kPa under a certain guaranteed rate.

As for the critical dynamic strength of filling, when the critical dynamic strength of subgrade filling is less than the dynamic stress generated by the dynamic train load, the soil structure will be destabilized, and the deformation will increase rapidly. However, when the situation is opposite, the soil is gradually compacted by load, and the increment of strain decreases gradually. If the load reaches a certain time, the soil density reaches a certain degree. Therefore, the actual dynamic stress is less than the critical dynamic strength, and the dynamic stress of the subgrade bed is stable for a long time. It was found that the minimum value of dynamic strength is 30 kPa even for the fine-grain soil, which is sensitive to water [31,71,72]. Additionally, the calculated method of the critical dynamic strength  $[\sigma_d]$  using foundation coefficient  $K_{30}$  or critical static strength  $[\sigma_0]$  was obtained [32] by analyzing the field data of subgrade of Da-Qin Line, which is shown in Equation (13) and Table 8. It can be seen that the calculated value is basically consistent with the measured value. According to the respective requirements of  $K_{30}$  for the filling at the subgrade bottom and the embankment below the subgrade bottom in “Code for Design of Railway Earth Structure” [12], the critical dynamic strength of filling at the subgrade bottom and the embankment below the subgrade bottom is, respectively, 147 kPa and 104 kPa.

$$[\sigma_d] = 0.45[\sigma_0] = 1.08K_{30} + 6.75 \quad (13)$$

**Table 8.**  $K_{30}$  and the critical dynamic strength of the corresponding subgrade filling.

The Type of Data	$K_{30}$ (MPa/m)	90	110	130	150	170	190
The calculated value	$[\sigma_0]$ (kPa)	231	279	327	375	425	471
	$[\sigma_d]$ (kPa)	104	126	147	169	190	212
The measured value	$[\sigma_d]$ (kPa)	118	134	150	166	182	199

The above analysis shows that the critical dynamic strength of subgrade filling is greater than the dynamic stress transferred to subgrade by the dynamic load. If the strength reduction coefficient of subgrade filling is determined, the dynamic stress in the subgrade structure layers needs to be determined. As is known, the dynamic stress of the subgrade bottom and embankment below the subgrade bottom is not fixed. According to the most unfavorable condition, the dynamic stress of subgrade bottom or the embankment top below the subgrade was taken to determine the strength criteria design of each layer filling: the dynamic stress  $\sigma_{dmax}$  of the subgrade bottom is 50 kPa, and the dynamic stress of embankment below the subgrade is 25 kPa.

#### 4.2. The Design Criteria

The filling strength design criteria of cement-stabilized loess could be obtained by substituting  $k_f$ ,  $\eta_G$ ,  $\eta_D$  and  $\sigma_{dmax}$  into Equation (3):

$$\text{The filling strength of subgrade bottom } \geq 50 / (0.26 \times 0.4 \times 0.3) = 1602 \text{ kPa}$$

$$\text{The filling strength of embankment below the subgrade } \geq 20 / (0.2 \times 0.4 \times 0.3) = 801 \text{ kPa}$$

The strength of cement-stabilized loess increases with age. 7-day strength is about 0.6 times the critical strength, while 90-day strength is about 0.9 times the critical strength [73,74]. There are at least 3 months between the completion of constructing subgrade and the beginning of train operation, so 90-day strength is too long to be used as the design index because it is not convenient for engineering application. The 7-day strength is usually used as the design index

in the project. Therefore, the 7-day strength design criterion was determined combined with the relationship between the strength and age of stabilized soil:

$$q_{u7} = (0.6 \times q_u) / 0.9 = \frac{2}{3} q_u \quad (14)$$

According to Equation (14), 7-day strength design criteria of cement-stabilized loess filling could be preliminarily obtained:

The filling strength of subgrade bottom  $\geq 1602 \text{ kPa} \times 2/3 = 1068 \text{ kPa}$ .

The filling strength of the embankment below the subgrade  $\geq 801 \text{ kPa} \times 2/3 = 534 \text{ kPa}$ .

Therefore, 7-day strength design criteria based on durability are presented, as shown in Table 9.

**Table 9.** The strength design criteria of cement-stabilized loess.

The Grade of Railway	7-Day Unconfined Compressive Strength Saturated with Water (kPa)	
	Subgrade Bottom	Embankment Below the Subgrade
Passenger and freight railway, Inter-city railway High-speed railway, Heavy-haul railway	$\geq 1100$	$\geq 550$

## 5. Conclusions

- (1) The effects of cement dosage and compaction level on the fatigue characteristics of cement-stabilized loess were investigated in this study. Taking into account the most unfavorable conditions, the strength fatigue reduction coefficient of 0.26 was obtained.
- (2) The effect of wet–dry cycling on the strength reduction of cement-stabilized loess was investigated in this study. The results show that the strength decreases continuously with the increase of the time of wet–dry cycling, and the strength became to be stable after 15 times. Taking into account the most unfavorable conditions, the strength reduction coefficient of cement-stabilized loess under wet–dry cycling of 0.40 was obtained.
- (3) The effect of freeze–thaw cycling on the strength reduction of cement-stabilized loess was investigated in this study. The results show that the strength decreases continuously with the increase of the time of freeze–thaw cycling, and the strength became to be stable after 12 times. Taking into account the most unfavorable conditions, the strength reduction coefficient of cement-stabilized loess under freeze–thaw cycling of 0.30 was obtained.
- (4) The dynamic stress level of the railway subgrade was analyzed in this study. Moreover, it was obtained that the dynamic stress  $\sigma_{dmax}$  of subgrade bottom is 50 kPa, and the dynamic stress  $\sigma_{dmax}$  of the embankment below the subgrade is 25 kPa.
- (5) The 7-day strength design criteria were presented based on durability: 7-day unconfined compressive strength of cement-stabilized loess saturated with water of the subgrade bottom should be higher than 1100 kPa, and 7-day unconfined compressive strength of cement-stabilized loess saturated with water of embankment below the subgrade should be higher than 550 kPa.

**Author Contributions:** F.W.: Conceptualization, Methodology, Formal analysis, Writing—Reviewing and Editing. W.P.: Methodology, Investigation, Data curation and Writing—original draft. L.H.: Conceptualization, Writing—original draft and Validation. Y.J.: Resources, Funding acquisition and Supervision. X.Q.: Visualization. All authors have read and agreed to the published version of the manuscript.

**Funding:** This research was funded by the Science and Technology Project of Shaanxi Provincial Department of Transportation (No. 18-02K and No. 19-27K), the Scientific Research of Central Colleges of China for Chang'an University (No. 300102218212), and the Science and Technology Project of Jilin Provincial Department of Transportation(2017ZDGC-7).

**Institutional Review Board Statement:** Not applicable.

**Informed Consent Statement:** Not applicable.

**Data Availability Statement:** Not applicable.

**Acknowledgments:** This research was supported by the Science and Technology Project of Shaanxi Provincial Department of Transportation (No. 18-02K and No. 19-27K), the Scientific Research of Central Colleges of China for Chang'an University (No. 300102218212), and the Science and Technology Project of Jilin Provincial Department of Transportation (2017ZDGC-7). The author gratefully acknowledges its financial support. Thanks to editors and reviewers for their efficient work.

**Conflicts of Interest:** The authors declare no conflict of interest.

## References

1. Chen, F. Foundations on expansive soils. *Dev. Geotech. Eng.* **1998**, *125*, 29–30.
2. Sumesh, M.; Kalita, A.; Singh, B. An experimental investigation on strength properties of fly ash blended soils treated with cement. *J. Environ. Res. Dev.* **2010**, *5*, 322–329.
3. Zhang, C.L.; Jiang, G.L.; Su, L.J.; Zhou, G.D. Effect of cement on the stabilization of loess. *J. Mt. Sci.* **2017**, *14*, 2325–2336. [[CrossRef](#)]
4. Ghadakpour, M.; Choobbasti, A.J.; Kutanaei, S.S. Experimental study of impact of cement treatment on the shear behavior of loess and clay. *Arab. J. Geosci.* **2020**, *13*, 1–11. [[CrossRef](#)]
5. Naeini, M.; Mohammadinia, A.; Arulrajah, A.; Horpibulsuk, S. Cyclic behavior of semi-rigid recovered plastic blends in railway track substructure. *Transp. Geotech.* **2021**, *28*, 100514. [[CrossRef](#)]
6. Naeini, M.; Mohammadinia, A.; Arulrajah, A.; Horpibulsuk, S. Recycled glass blends with recycled concrete aggregates in sustainable railway geotechnics. *Sustainability* **2021**, *13*, 2463. [[CrossRef](#)]
7. Lee, F.H.; Lee, Y.; Chew, S.H. Strength and modulus of marine clay-cement mixes. *J. Geotech. Geoenviron. Eng.* **2005**, *131*, 178–186. [[CrossRef](#)]
8. Consoli, N.C.; Foppa, D.; Festugato, L.; Heineck, K.S. Key parameters for strength control of artificially cemented soils. *J. Geotech. Geoenviron. Eng.* **2007**, *133*, 197–205. [[CrossRef](#)]
9. Gallavresi, F. Grouting improvement of foundation soils. In *Grouting, Soil Improvement and Geosynthetics*; American Society of Civil Engineers (ASCE): New York, NY, USA, 1992; pp. 1–38.
10. China Iron Fourth Bureau Group Co. Ltd. *Technical Regulation of Improved Soil for Railway Subgrade (Draft Submitted)*; China Iron Fourth Bureau Group Co. Ltd.: Anhui, China, 2007. (In Chinese)
11. Sun, M.Z.; Guo, S.Y. *Research on Improvement Technology of Heavy-Haul Railway Subgrade Filling*; The Third Railway Survey and Design Institute: Tianjin, China, 2005. (In Chinese)
12. National Railway Administration. *Code for Design of Railway Earth Structure*; China Railway Press: Beijing, China, 2016. (In Chinese)
13. Zhu, Z.Y.; Ling, X.Z.; Chen, S.J.; Zhang, F.; Wang, Z.Y.; Wang, L.N.; Zou, Z.Y. Analysis of dynamic compressive stress induced by passing trains in permafrost subgrade along Qinghai-Tibet Railway. *Cold Reg. Sci. Technol.* **2011**, *65*, 465–473. [[CrossRef](#)]
14. Yao, H.L.; Hu, Z.; Wang, H. Analytical model to predict dynamic responses of railway subgrade due to high-speed trains considering wheel-track interaction. *Int. J. Geomech.* **2016**, *16*, 1–15. [[CrossRef](#)]
15. Wang, T.; Luo, Q.; Zhang, L.; Xiao, S.; Fu, H. Dynamic response of stabilized cinder subgrade during train passage. *Constr. Build. Mater.* **2021**, *270*, 121370. [[CrossRef](#)]
16. Ma, X.; Zhang, Z.; Zhang, P.; Wang, X. Long-term dynamic stability of improved loess subgrade for high-speed railways. *Proc. Inst. Civil Eng. Geotech. Eng.* **2020**, *173*, 217–227. [[CrossRef](#)]
17. Fang, R.; Lu, Z.; Yao, H.; Luo, X.; Yang, M. Study on dynamic responses of unsaturated railway subgrade subjected to moving train load. *Soil Dyn. Earthq. Eng.* **2018**, *115*, 319–323. [[CrossRef](#)]
18. Hu, P.; Zhang, C.; Wen, S.; Wang, Y. Dynamic responses of high-speed railway transition zone with various subgrade fillings. *Comput. Geotech.* **2019**, *108*, 17–26. [[CrossRef](#)]
19. Chen, J.; Zhou, Y. Dynamic responses of subgrade under double-line high-speed railway. *Soil Dyn. Earthq. Eng.* **2018**, *110*, 1–12. [[CrossRef](#)]
20. Mei, H.; Leng, W.; Nie, R.; Tu, R.; Li, Y.; Dong, J. Experimental research on the dynamic response characteristics of the transition subgrade induced by heavy-haul train passage. *Proc. Inst. Mech. Eng. Part F* **2019**, *233*, 974–987. [[CrossRef](#)]
21. Cai, Y.; Xu, L.; Liu, W.; Shang, Y.; Su, N.; Feng, D. Field test study on the dynamic response of the cement-improved expansive soil subgrade of a heavy-haul railway. *Soil Dyn. Earthq. Eng.* **2020**, *128*, 105878. [[CrossRef](#)]

22. Wenjie, L.; Wuming, L.; Xiaowei, W.; Chunyan, Z.; Qi, Y. Numerical simulation analysis on dynamic stress of railway subgrade under heavy haul condition. In Proceedings of the 8th International Conference on Intelligent Computation Technology and Automation (ICICTA), Nanchang, China, 14–15 June 2015; pp. 592–596.
23. Mei, H.; Leng, W.; Nie, R.; Liu, W.; Chen, C.; Wu, X. Random distribution characteristics of peak dynamic stress on the subgrade surface of heavy-haul railways considering track irregularities. *Soil Dyn. Earthq. Eng.* **2019**, *116*, 205–214. [[CrossRef](#)]
24. Li, J.; Chen, S.; Yu, F.; Dai, Z. Remote monitoring for a high-speed railway subgrade structure state in a mountainous area and its response analysis. *Bull. Eng. Geol. Environ.* **2017**, *77*, 409–427. [[CrossRef](#)]
25. Ye, Y.S.; Cheng, A.J.; Zhang, Q.L. Study on the design and compaction criteria of improved soil subgrade. *China Railw. Sci.* **2008**, *29*, 1–5. (In Chinese)
26. Wang, W.Q.; Liu, B.X.; Wang, Y.Q. The attenuating rule of dynamic-load stress along the depth of high-speed railroad roadbed. *J. Xihua Univ. Nat. Sci.* **2008**, *27*, 98–111. (In Chinese)
27. Shang, Y.H.; Yin, F.F.; Xu, L.R.; Chen, Z. Numerical research on the dynamic features of cement-stabilized expansive soil subgrade of heavy haul railway. *Railw. Criteria Des.* **2020**, *64*, 18–23. (In Chinese)
28. Zhao, F.L.; Zhang, J. Study on evaluation and test of road base of existing railway. *J. Railw. Eng. Soc.* **2011**, *28*, 15–21. (In Chinese)
29. Liu, H. Study on attenuation law of dynamic stress along depth of high-speed railway subgrade. *Sichuan Build. Mater.* **2011**, *37*, 172–175. (In Chinese)
30. Dong, J.; Yang, Y.; Zhang, X.S.; Ma, Y.Y. Study on dynamic response of different improvement thickness of subgrade bed of heavy haul railway. *Railw. Criteria Des.* **2019**, *63*, 33–39. (In Chinese)
31. Dong, L.; Zhao, C.G.; Cai, D.G.; Zhang, Q.L.; Ye, Y.S. Method for dynamic response of subgrade subjected to high-speed moving load. *Eng. Mech.* **2008**, *25*, 231–240. (In Chinese)
32. Lv, W.Q. Study of Subgrade Structure Design Theory and Key Technology on Heavy Haul Railway of Large Axle Load. Master's Thesis, Southwest Jiaotong University, Chengdu, China, 2012. (In Chinese).
33. Peng, W.; Hang, H.X. On calculation methods for subgrade dynamic stress of railway subgrade and its attenuation law along depth. *Shanxi Archit.* **2010**, *36*, 286–287. (In Chinese)
34. Kong, X.H.; Jiang, G.L.; Zou, Z.Y. Experimental study on dynamic response of subgrade bed of high-speed railway. *Railw. Eng.* **2013**, *77*–81. (In Chinese)
35. Liu, J.L.; Ye, Q.Z.; Song, X.G.; Luo, Q.; Lv, W.Q. Study on stress and deformation analytic method of heavy haul railway subgrade based on transfer-matrix. *Railw. Criteria Des.* **2014**, *58*, 14–19. (In Chinese)
36. Wang, R. The Dynamic Response and Long-Term Strength and Settlement of Loess Railway Embankment Subjected to Train Load. Ph.D. Thesis, Chang'an University, Xi'an, China, 2019. (In Chinese).
37. Fahoum, K.; Aggour, M.S.; Amini, F. Dynamic properties of cohesive soils treated with lime. *Geotech. Geoenviron. Eng.* **1996**, *122*, 382–389. [[CrossRef](#)]
38. Preteseille, M.; Lenoir, T. Mechanical fatigue behavior in treated/stabilized soils subjected to a uniaxial flexural test. *Int. J. Fatigue* **2015**, *77*, 41–49. [[CrossRef](#)]
39. Lenoir, T.; Preteseille, M.; Ricordel, S. Contribution of the fiber reinforcement on the fatigue behavior of two cement-stabilized soils. *Int. J. Fatigue* **2016**, *93*, 71–81. [[CrossRef](#)]
40. Zhou, Z.; Ma, W.; Zhang, S.; Mu, Y.; Li, G. Effect of freeze-thaw cycles in mechanical behaviors of frozen loess. *Cold Reg. Sci. Technol.* **2018**, *146*, 9–18. [[CrossRef](#)]
41. Wang, F.; Li, G.; Ma, W.; Mu, Y.; Zhou, Z.; Zhang, J.; Chen, D.; Zhao, J. Effect of repeated wetting-drying-freezing-thawing cycles on the mechanic properties and pore characteristics of compacted loess. *Adv. Civ. Eng.* **2020**, 8839347. [[CrossRef](#)]
42. Zhang, Y.; Johnson, A.E.; White, D.J. Freeze-thaw performance of cement and fly ash stabilized loess. *Transp. Geotech.* **2019**, *21*, 100279. [[CrossRef](#)]
43. Xu, J.; Wang, X.; Ren, J.; Yuan, J. Mechanism of shear strength reduction of loess during freeze-thaw cycling. *Geomech. Eng.* **2018**, *14*, 307–314.
44. She, H.; Hu, Z.; Qu, Z.; Li, H.; Guo, H.; Ma, X. Structural strength reduction characteristics and a model of undisturbed loess under the action of wetting and freeze-thaw cycles. *Math. Probl. Eng.* **2019**, *2019*, 4790250. [[CrossRef](#)]
45. Bi, G.Q. Study on influence of freeze-thaw cycles on the physical-mechanical properties of loess. *Adv. Mater. Res.* **2012**, *442*, 286–290. [[CrossRef](#)]
46. Li, G.; Wang, F.; Ma, W.; Fortier, R.; Mu, Y.; Mao, Y.; Hou, X. Variations in strength and deformation of compacted loess exposed to wetting-drying and freeze-thaw cycles. *Cold Reg. Sci. Technol.* **2018**, *151*, 159–167. [[CrossRef](#)]
47. Yan, C.G.; Zhang, Z.Q.; Jing, Y.L. Characteristics of strength and pore distribution of lime-flyash loess under freeze-thaw cycles and dry-wet cycles. *Arab. J. Geosci.* **2017**, *10*, 1–10. [[CrossRef](#)]
48. Yan, C.; An, N.; Wang, Y.; Sun, W. Effect of dry-wet cycles and freeze-thaw cycles on the antierosion ability of fiber-reinforced loess. *Adv. Mater. Sci. Eng.* **2021**, 8834598. [[CrossRef](#)]
49. Hu, C.M.; Yuan, Y.L.; Mei, Y.; Wang, X.Y.; Liu, Z. Comprehensive strength reduction model of compacted loess exposed to drying-wetting cycles. *Bull. Eng. Geol. Environ.* **2020**, *79*, 383–398. [[CrossRef](#)]
50. Zhang, Z.J.; Tao, M.J. Durability of cement stabilized low plasticity soils. *J. Geotech. Geoenviron. Eng.* **2008**, *134*, 203–213. [[CrossRef](#)]
51. Helson, O.; Eslami, J.; Beaucoeur, A.L.; Noumowe, A.; Gotteland, P. Durability of soil mix material subjected to wetting/drying cycling and external sulfate attacks. *Constr. Build. Mater.* **2018**, *192*, 416–428. [[CrossRef](#)]

52. Zhao, A.P.; Tang, A.P.; Sun, J.; Yu, X.M. Tests and research on characteristics of shear strength of cement improved soil under freeze-thaw cycling. *Adv. Mater. Res.* **2014**, *1015*, 105–109. [[CrossRef](#)]
53. National Railway Administration. *Code for Soil Test of Railway Engineering (TB 10102-2010)*; China Railway Press: Beijing, China, 2010. (In Chinese)
54. Huang, S.G. Dynamic Response Research and Cumulative Settlement Control Analysis of Embankment-Cut Transition Section of Heavy Haul Railway in Loess Region. Ph.D. Thesis, Beijing Jiaotong University, Beijing, China, 2019. (In Chinese).
55. Jiang, Y.J.; Wang, H.Y.; Qiao, H.Y.; Yue, W.M.; Dong, X. Stability of cement-stabilized loess subgrade under water, wet-dry and freezing-thawing cycling. *Sci. Technol. Eng.* **2020**, *20*, 14592–14599. (In Chinese)
56. Research Institute of Highway Ministry of Transport. *Testing Methods of Material Stabilized with Inorganic Binders for Highway Engineering (JTG E51-2009)*; China Communications Press: Beijing, China, 2009. (In Chinese)
57. Jiang, Y.J.; Zhao, Z.L.; Li, M.J. Fatigue characteristics of asphalt mixture designed by two methods. *J. Jiangsu Univ.* **2016**, *37*, 473–478. (In Chinese)
58. Zhu, J.H.; Zhu, X.B.; Meng, D.Y.; Zhang, S.H.; Jiang, Y.J. Study on fatigue characteristics of cement stabilized macadam compacted by vertical vibration. *Road Mach. Constr. Mech.* **2019**, *36*, 40–45. (In Chinese)
59. Romanov, V. Experimental Investigation on Permanent Deformation of Ballast-Coarse Grained Soil Induced by Cyclic Train Load. Master's Thesis, Harbin Institute of Technology, Harbin, China, 2016. (In Chinese).
60. Zhang, R.G. Exploration of design technique on substructure for 400 km/h high-speed railway and 40t axle-load heavy haul railway. Master's Thesis, Southwest Jiaotong University, Chengdu, China, 2017. (In Chinese).
61. Zhou, Y.W. *Chinese Tundra*; Science Press: Beijing, China, 2000. (In Chinese)
62. Ding, J.K. *Permafrost and Railway Engineering*; China Railway Press: Beijing, China, 2011. (In Chinese)
63. Han, Z.L.; Zhang, Q.L. Dynamic stress analysis on speed-increase subgrade of existing railway. *China Railw. Sci.* **2005**, *26*, 1–5. (In Chinese)
64. Qu, X.H.; Cui, J.J. *Railway Subgrade Design Technology for Passenger Dedicated Line*; China Communications Press: Beijing, China, 2008. (In Chinese)
65. Zhan, Y.X. Study on Design Method of Pile-Plank Embankment of Ballastless Track in High-Speed Railway by Tests. Ph.D. Thesis, Southwest Jiaotong University, Chengdu, China, 2007. (In Chinese).
66. Wu, H.H. Research on Dynamics of 30t Axle Load Heavy Haul Train on the Mengxi-Central China Railway. Master's Thesis, Southwest Jiaotong University, Chengdu, China, 2017. (In Chinese).
67. Jia, J.Z. Dynamic load characteristics of heavy-haul railway subgrade. *Railw. Eng.* **2014**, *7*, 89–91. (In Chinese)
68. Ye, Y.S. Dynamic response performance of high-speed railway subgrade. *Railw. Eng.* **2015**, *10*, 7–12. (In Chinese)
69. National Railway Administration. *Code for Design of Intercity Railway (TB 10623-2014)*; China Railway Press: Beijing, China, 2014. (In Chinese)
70. National Railway Administration. *Code for Design of High-Speed Railway (TB 10621-2014)*; China Railway Press: Beijing, China, 2014. (In Chinese)
71. Xia, M.X. Dynamic characteristics of cement improved soil as high-speed railway subgrade. *Value Eng.* **2013**, *32*, 100–101. (In Chinese)
72. Zhang, P.Y.; Ma, X.N.; Li, S.Z.; Wang, X. Long-term dynamic stability evaluation for cement-improved loess subgrade of high-speed railway. *J. Vib. Shock.* **2019**, *38*, 80–87. (In Chinese)
73. Jiang, Y.J.; Yuan, K.J.; Li, Q.L. Comparison of mechanical properties of cement-stabilized loess produced using different compaction methods. *Adv. Mater. Sci. Eng.* **2020**, *2020*, 4835704. [[CrossRef](#)]
74. Jiang, Y.; Li, Q.; Yi, Y.; Yuan, K.; Deng, C.; Tian, T. Cement-stabilized loess base for intercity railways: Mechanical strength and influencing factors based on the vertical vibration compaction method. *Materials* **2020**, *13*, 3643. [[CrossRef](#)] [[PubMed](#)]